Supplement of Hydrol. Earth Syst. Sci., 27, 3463–3484, 2023
https://doi.org/10.5194/hess-27-3463-2023-supplement

Hydrology and Earth System Sciences
Open Access
EGU

Supplement of

Spatial distribution and controls of snowmelt runoff in a sublimation-dominated environment in the semiarid Andes of Chile

Álvaro Ayala et al.

Correspondence to: Álvaro Ayala (alvaro.ayala@ceaza.cl)

Supplement

Section S1: Discriminating sensor noise from actual precipitation

As the original cumulative precipitation record (at an hourly time scale) is a noisy record, it is difficult to identify actual precipitation events from the noise. To overcome this problem, we followed this procedure:

- We averaged the hourly records of cumulative precipitation to daily means.
- We identified days with an increase (P) in the cumulative record.
- At each of those days, we compared the average of the previous five days (Pb) with the average of the following five days (Pf). If Pf > Pb + PT then we assumed that P corresponded to an actual precipitation event. PT is a threshold to be calculated.
- To determine PT, we calculated the number of days on which the albedo and snow height records at TAP increased. We interpreted those increases as days with precipitation. We then compared the number of events from those records against the number of events from the precipitation records. We chose PT as the number that minimizes the average error in that comparison. We obtained a value of 6 mm/day.
- Finally, we distributed daily precipitation to hourly values using the hourly distribution from the cumulative precipitation record.

Section S2: Supplementary images and tables

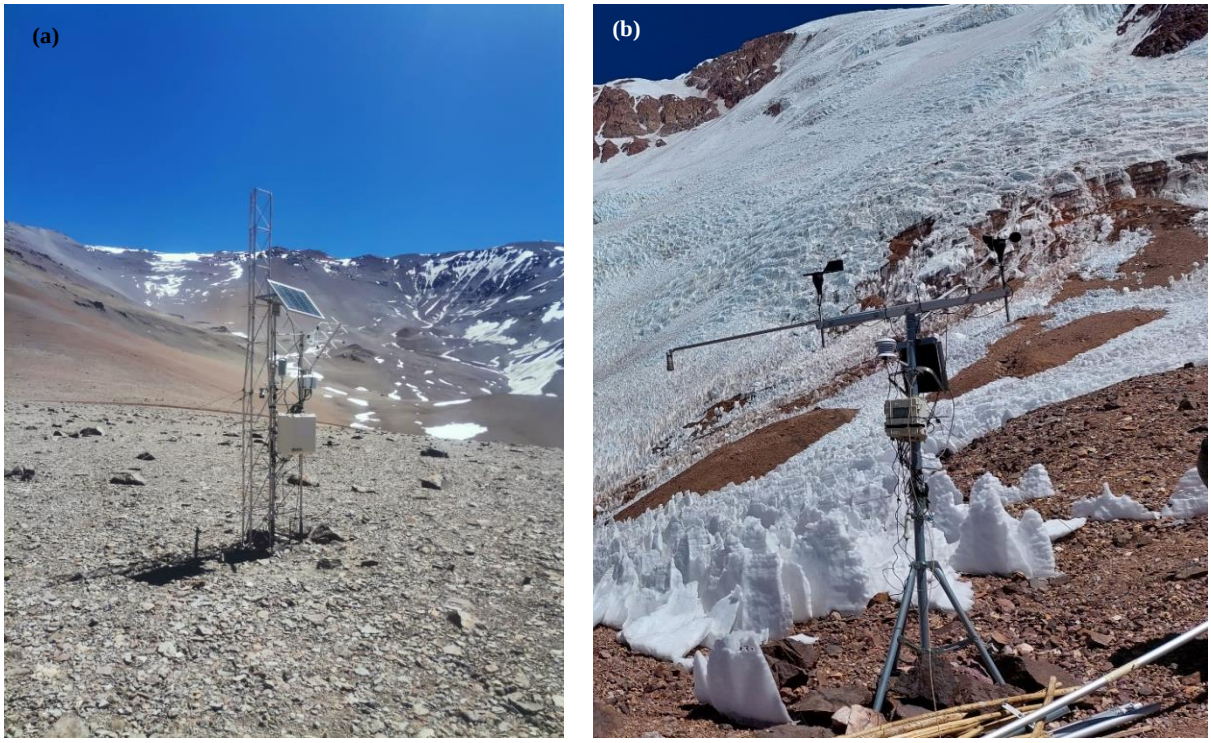

Figure S1: (a) Paso Agua Negra (PAN), and (b) Tapado Glacier (TGL) Automatic Weather Stations.

Ablation stakes network

The stakes were manually drilled on the ablation zone of the glacier and were visited approximately every month during the ablation season (Figure S2 and Table S1). The visit and maintenance of the ablation stakes was difficult due to the development of snow and ice penitentes of 3-4 m height (Figure S3), which also led to the collapse of some monitored sites. Penitentes are cone-shaped snow and ice structures formed in dry environments by differential ablation rates along their height (Lliboutry, 1954). The ablation stakes network consists of traditional single-point measurements and one site where we registered geometry changes around the stake to account for the differential ablation of the surface associated with the penitentes (Rivera et al., 2016).

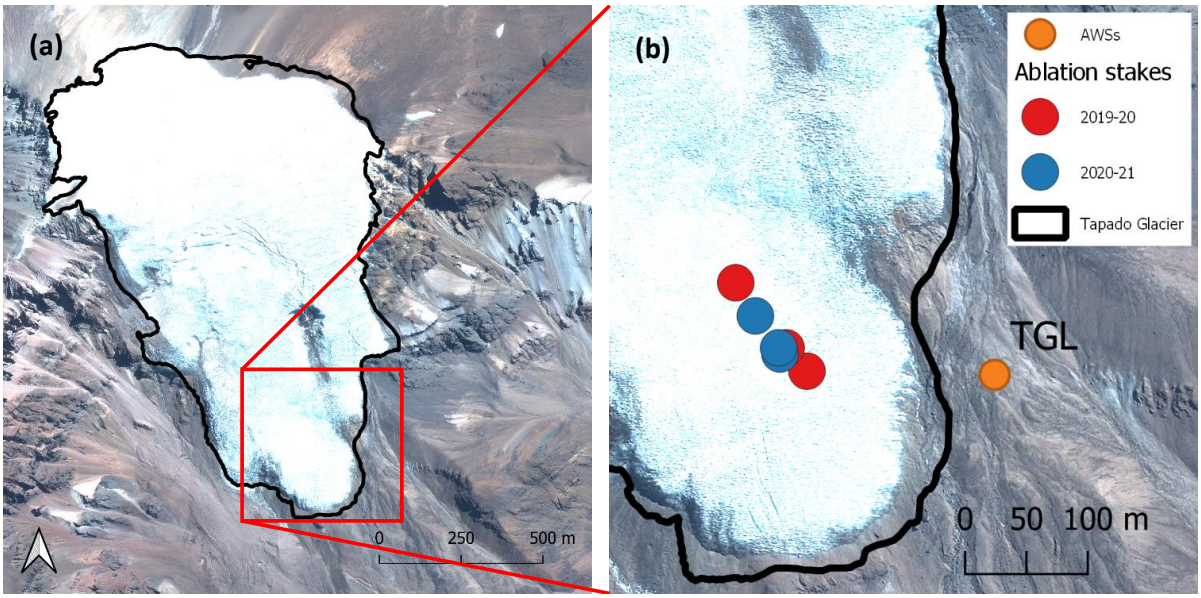

Figure S2: Ablation stakes on Tapado Glacier. (a) Map of ablation stakes, (b-d) Images of ablation stakes. Background imagery is a Pléiades scene from 2020, © CNES (2018) and Airbus DS (2018), all rights reserved.

Figure S3: Images of ablation stakes and penitentes on Tapado Glacier. (a) Ablation stake in summer 2020, (b) Ablation stake in summer 2021, (c) and (d) 3-4 m penitentes in summer 2021.

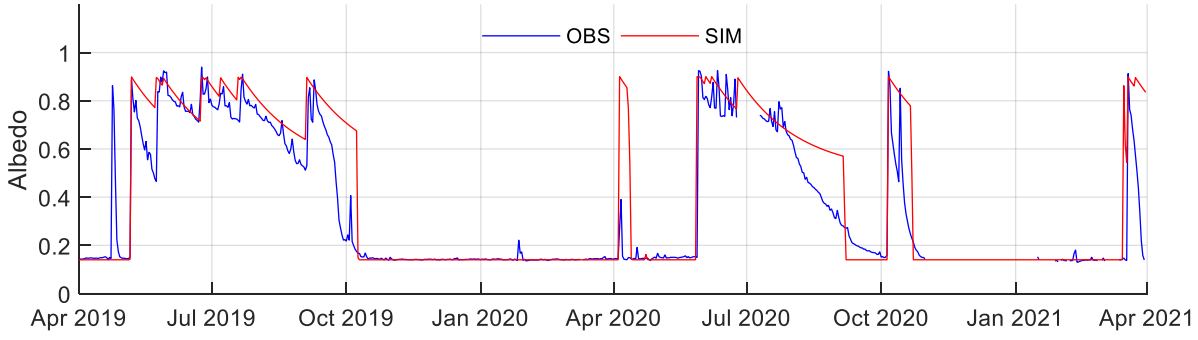

Figure S4: Simulated and observed albedo at TAP after the manual adjustment of the albedo decay parameters (see Table 3).

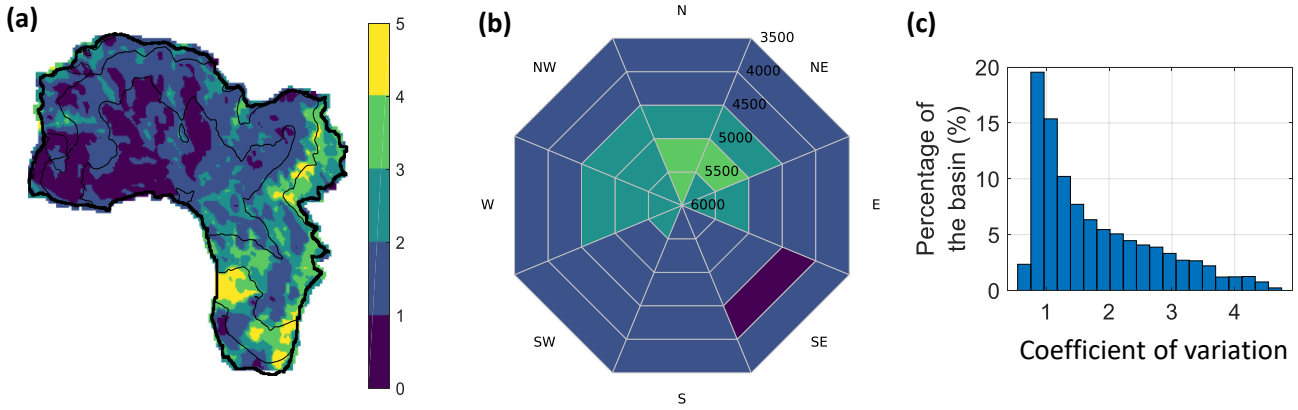

Figure S5: Coefficient of variation of the annual maximum snow accumulation in the Corrales basin during 1985-2015 according to the daily SWE reconstruction by Cortés and Margulis (2017)**. (a) Map of the coefficient of variation, (b) Polar plot of the coefficient of variation, (c) Histogram of the coefficient of variation, Glaciers outlines and contour lines are shown in (a).**

In Figure S6 we compare simulated values of surface mass balance on the lowest section of the debris-free Tapado Glacier (below 4800 m a.s.l.) against the set of ablation stakes readings (Section 3.1). The surface glacier mass balance of this area is calculated using snow accumulation and erosion (snowfall and wind transport), snow ablation (surface sublimation, blowing snow sublimation and snowmelt runoff) and ice melt and sublimation. As the ablation measured at the stakes and that of their corresponding model grid cells might differ due to topographic differences between the sites and that of the 50-m resolution DEM, we prefer to compare all the stakes readings against spatially averaged values over the glacier tongue.

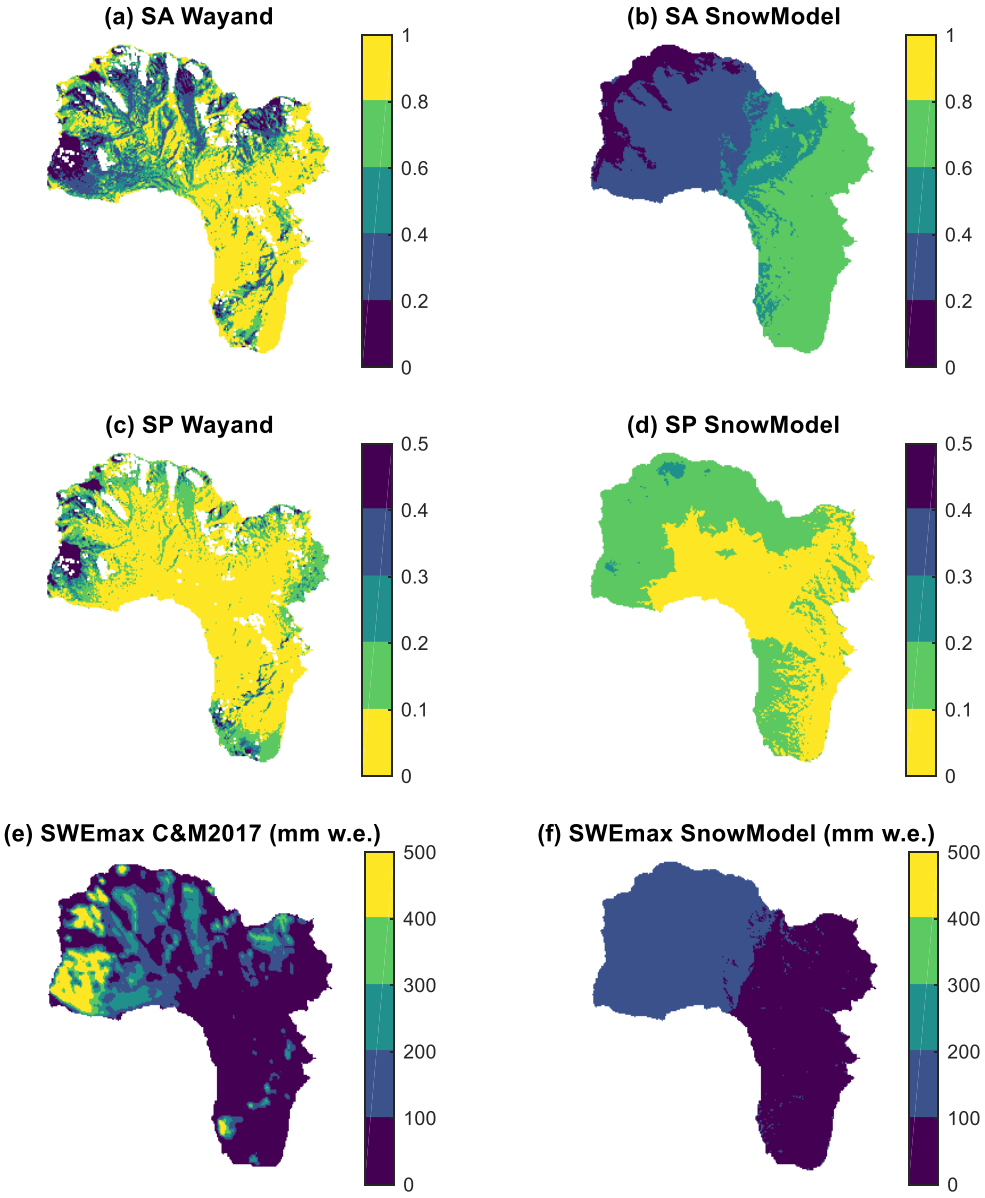

Figure S6: Comparison of reference and simulated snow products (SA, SP and SWEmax) as in Figure 5b-d but using maps.

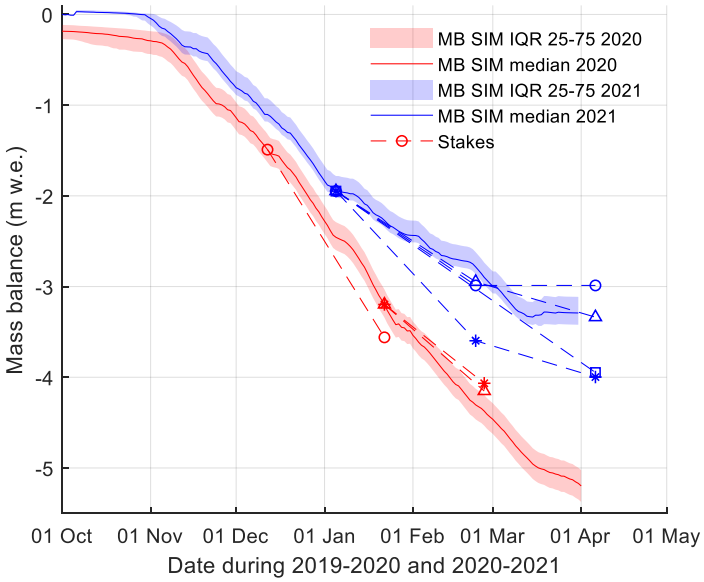

Figure S7: Comparison of the simulated cumulative mass balance of the ablation area of Tapado Glacier against ablation stakes readings in the period October-April of years 2019-2020 and 2020-2021. The red and blue lines and areas represent the median values and interquartile ranges 25 and 75 of the SnowModel ensemble runs, respectively. The markers correspond to the ablation stakes readings and the dashed lines are connecting lines that help visualization. To help comparison, we set the first marker of each line at the simulated mass balance value in that date. The cumulative mass balance is set at zero on April 1 of each year.

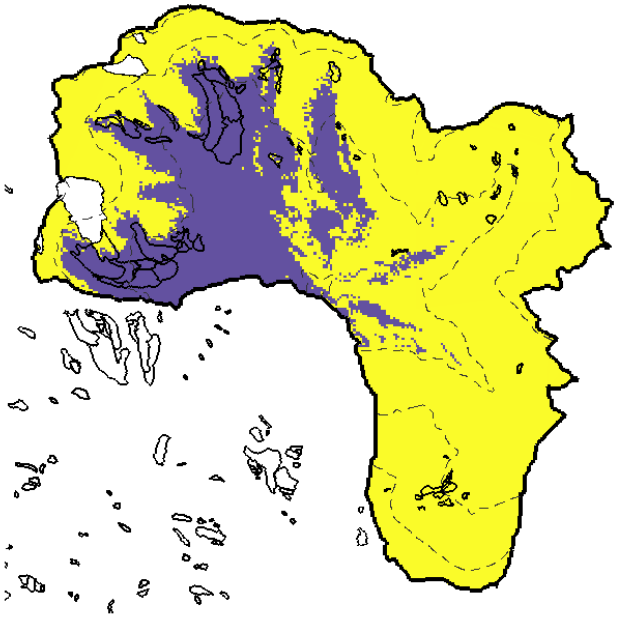

Figure S8: Snowmelt hotspots as in Figure 10b but adding the outlines of rock glaciers in the study area. Clean glaciers in the catchment are shown in white.

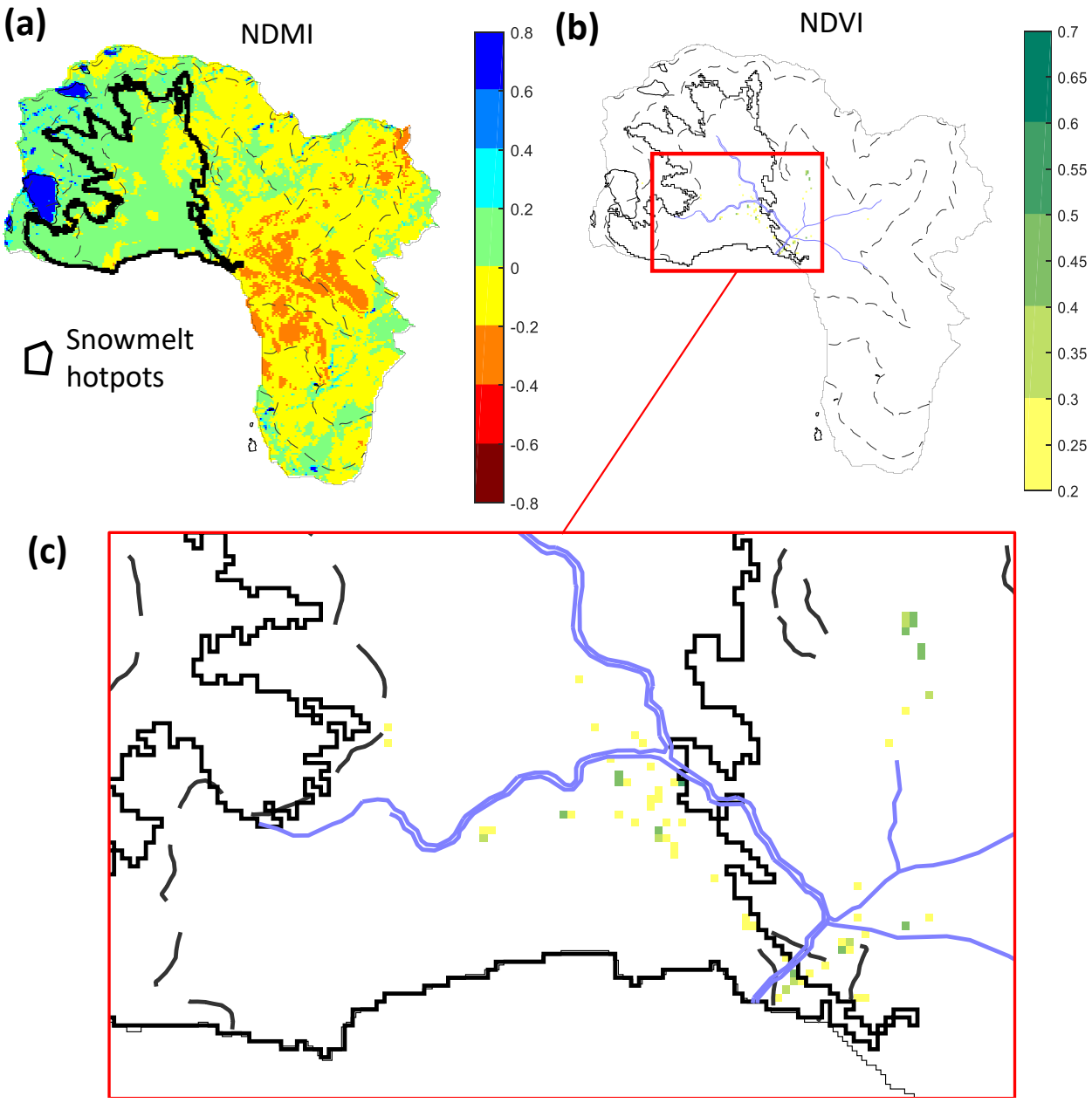

Figure S9: (a) Normalized Difference Moisture Index (NDMI) and (b) Normalized Difference Vegetation Index (NDVI) of the Corrales catchment in the period 15-12-2019 and 15-01-2020. (c) Zoom to the riparian areas using the NDVI map. The maps were calculated using the average NDMI and NDVI from six available Sentinel 2 Level 2A images for that period.

Table S1: Location of Tapado Glacier ablation stakes

Stake	East	South	Elevation	Year
1	410968	6664161	4765	2019-2020
2	410951	6664180	4794	2019-2020
3	410910	6664233	4761	2019-2020
4 (with geometry changes)	410946	6664175	4754	2020-2021
5	410945	6664180	4756	2020-2021
6	410926	6664206	4766	2020-2021

Table S2: List of satellite images used for the calculation of the snow indices (SA and SP)

Index	Product	Number of images	Dates (YYYYMMDD)
SA	Landsat 8	18	20190413, 20190429, 20190515, 20190616, 20190702, 20190718, 20190803, 20190819, 20190904, 20190920, 20200415, 20200501, 20200517, 20200602, 20200805, 20200821, 20200906, 20200922
	Sentinel 2	15	20190603, 20190623, 20190703, 20190718, 20190728, 20190827, 20190827, 20200408, 20200408, 20200418, 20200523, 20200528, 20200702, 20200806, 20200910
SP	Landsat 8	21	20191006, 20191107, 20191123, 20191209, 20191225, 20200110, 20200126, 20200211, 20200227, 20200314, 20200330, 20201008, 20201024, 20201109, 20201125, 20201211, 20201227, 20210112, 20210128, 20210213, 20210317
	Sentinel 2	23	20191115, 20191115, 20191120, 20200104, 20200104, 20200119, 20200119, 20200124, 20200124, 20200304, 20200304, 20201015, 20201209, 20210118, 20210118, 20210123, 20210123, 20210128, 20210212, 20210227, 20210304, 20210304, 20210314